The axial wave equivalent to a group of interfering modes in underwater acoustics

Natalie Grigorieva and Gregory Fridman

Department of Applied Mathematics and Mathematical Modeling, St. Petersburg State Marine Technical University,
3 Lotsmanskaya str., 190008, St. Petersburg, Russia,
nsgrig@natalie.spb.su **grifri@peterlink.ru**

A series of long-range, low-frequency, ocean propagation experiments conducted since the mid 1980's attest to the complex nature of near-axial propagation in a deep-water waveguide. The most pronounced characteristics of the time-of-arrival patterns for these experiments are early geometrical-like arrivals followed by a crescendo of energy that propagates along the axis. It is impossible to explain this late-arriving energy using the geometrical acoustics because of the presence of cusped caustics repeatedly along the axis. The neighborhoods of interference grow with range and at long ranges they overlap producing a special "axial wave" that propagates along the axis like a wave. In this paper for an arbitrary two-dimensional underwater sound channel the axial wave is represented in the form of a sum of the first normal modes and a remainder field. The mathematical framework is provided by two different representations of the acoustic field. The first one includes a sum of ray summands and the axial wave. The second representation consists of ray summands, a sum of the first normal modes, and a remainder field. Numerical simulations are carried out for the Munk canonical sound-speed profile in the range interval $[1600; 1650]$ km at the frequency of 200 Hz.

1 Introduction

In many long-range propagation experiments the source and receiver are placed close to the depth of the sound-channel (SOFAR) axis to minimize the interaction of the acoustic field with the ocean's surface and bottom. All these experiments are consistent in their description of the time-of-arrival patterns of the received signal. They include early, resolvable, geometrical-like intensity peaks followed by the axial crescendo of unresolved energy. The early intensity peaks can be unambiguously identified with acoustic energy that propagates along ray paths calculated for ocean models that are reasonable representations of the ocean conditions. The axial crescendo consists of a jagged buildup of the acoustic energy with time to a relatively high peak followed by a rapid termination of the signal. In Fig. 1 these characteristics are clearly shown for a time-of-arrival pattern measured during the Acoustic Engineering Test (AET) for the Acoustic Thermometry of Ocean Climate (ATOC) program. This figure is adapted from one published in [1]. The axial crescendo accumulates an essential part of energy of the received signal, but it is unknown how to extract from it the useful information about the ocean conditions.

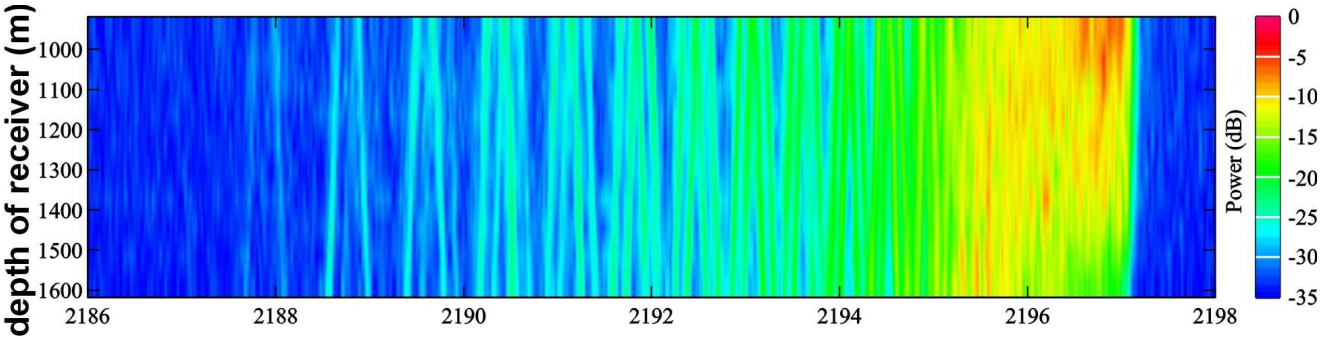

Fig. 1: One of time-of-arrival patterns measured during the AET experiment.

While the eikonal equation can be solved for the ray paths and travel times can be calculated by integrating along these paths, applications to use the geometrical acoustics to describe the propagation of energy along the waveguide axis entail difficulties resulting from the existence of cusped caustics repeatedly along the axis. Figure 2 illustrates this pattern of caustics. This is a ray tracing for a source on the axis (and for relatively short ranges). In neighborhoods of cusped caustics the very complicated interference processes are observed. They are described by the Pearcey integral [2].

The longitudinal and transverse sizes of the neighborhood of a cusp of a caustic, where simple ray acoustics formulas are not applicable, increase with range. As a result, at the certain propagation range the neighborhoods of adjacent cusps overlap. In this case the acoustic field cannot be described by the Pearcey integral and the more complicated interference structure appears. Therefore, a study of the axial crescendo when the geometrical solution is characterized by a multitude of cusped caustics should include an investigation of the interference of near-axial waves.

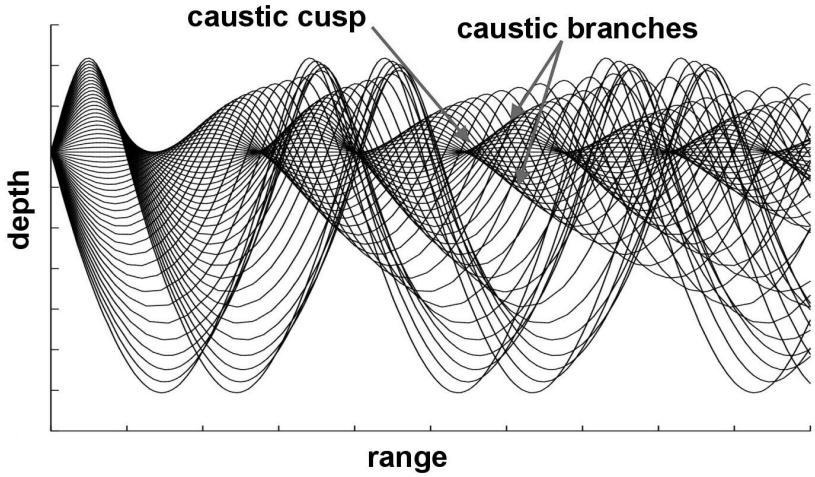

Fig. 2: Ray tracing for a source on the axis of the waveguide.

For a very idealized model of a symmetric waveguide, Buldyrev [3] showed that the interference of the wave fields that correspond to near-axial rays, and is associated with the cusped caustics, leads to formation of a coherent structure (the axial wave) that propagates along the axis like a wave. For an arbitrary range-independent underwater waveguide the formula for the axial wave was obtained by Grigorieva and Fridman [4]. It was generalized to the case of a range-dependent ocean in [5].

The purpose of this paper is to obtain for a range-independent medium model the representation of the axial wave in the form of a sum of the first modes and a remainder field that will provide an opportunity to understand better the interference structure of the acoustic field near the axis of an underwater sound channel in a deep-water sea.

The mathematical framework is provided by two different representations of the acoustic field. The first one was obtained in [4]. It includes a sum of ray summands and the axial wave. The second representation of the acoustic field is derived in the present paper. It includes ray summands, a sum of the first normal modes, and a remainder field. For a simple medium model with the parabolic index of refraction squared the desired representation of the axial wave was obtained in [6].

2 Integral representation of the wave field

For simplicity we consider the situation where the wave field depends on two spatial coordinates: the range coordinate, X, and the depth coordinate, Z, which is measured relatively to the depth of the sound-channel axis. We suppress the dependence of the field on the time factor $\exp(-\mathrm{i}\omega t)$, where ω is a cyclic frequency and t is the time.

In this paper we will study the interference of the wave travelling directly along the sound-channel axis with the wave fields corresponding to the rays with small launch angles. These rays do not reach the ocean's surface and bottom what allows the use of the model of an infinite ocean.

It is assumed that the sound speed $c(Z)$ can be expanded in the case of small Z in the form

$$c(Z) = c_0 + \frac{c_2}{2!}\,Z^2 + \frac{c_3}{3!}\,Z^3 + \ldots, \quad c_2 > 0 \qquad (1)$$

and when $Z \to \pm\infty$, the sound speed tends to the constants $c_\infty^{\pm} > c_0$. Since in Eq. (1), $c_1 = c'(0) = 0$ and $c_2 = c''(0) > 0$, the acoustic propagation in the ocean is characterized by the formation of a deep-water waveguide with the sound-channel axis $Z = 0$.

Let $X = 0$ and $Z = Z_0$ be the coordinates of the source. We introduce dimensionless coordinates $x = X/a$, $z = Z/a$, where $a = \sqrt{c_0/c_2}$ is the characteristic dimension of the waveguide, and a dimensionless wave number $\kappa = (\omega/c_0)\,a$.

The standard formulation of the problem is given by the wave equation

$$\frac{\partial^2 U_j}{\partial x^2} + \frac{\partial^2 U_j}{\partial z^2} + \kappa^2\, n^2(z)\, U_j = 0\,, \qquad (2)$$

where $n(z) = c_0/c(a\,z) = 1 - n_2\,z^2 + n_3\,z^3 + \ldots\, n_2 > 0$ is the index of refraction and the functions $U_j(x,z)$, $j = 1, 2$ are the wave fields above and below the depth of the source,

respectively. The equation (2) is supplemented with the continuity condition at the depth of the source

$$U_1(x, z_0) = U_2(x, z_0) \,, \tag{3}$$

where $z_0 = Z_0/a$, the discontinuity condition at the horizontal location of the source

$$\left(\frac{\partial U_1}{\partial z} - \frac{\partial U_2}{\partial z} \right) \Big|_{z=z_0} = 2\pi\, \delta(x) \,, \tag{4}$$

where $\delta(x)$ is the Dirac delta-function, and the radiation condition at infinity as $r \equiv \sqrt{x^2 + z^2} \to \infty$, $\operatorname{Im} \kappa > 0$

$$U_j(x, z) \to 0 \,. \tag{5}$$

Let us denote via $\Phi_1(z, \zeta)$ and $\Phi_2(z, \zeta)$ two linearly independent solutions of the equation

$$\frac{d^2\Phi}{dz^2} + \kappa^2 \left(n^2(z) - \zeta^2 \right) \Phi = 0 \tag{6}$$

satisfying the conditions

$$\begin{aligned} &\Phi_1(z, \zeta) \to 0 \quad \text{as} \quad z \to -\infty \,; \\ &\Phi_2(z, \zeta) \to 0 \quad \text{as} \quad z \to +\infty \,. \end{aligned} \tag{7}$$

$W(\zeta)$ is the Wronskian of these solutions. Fourier transforming in the range variable and using the method of separation of variables in (2)–(5) gives:

$$U_j(x_r, z_r; z_0) = \kappa \int\limits_{-\infty}^{\infty} \frac{\Phi_l(z_0, \zeta)\, \Phi_j(z_r, \zeta)}{W(\zeta)}\, \mathrm{e}^{\mathrm{i}\,\kappa\, x_r\, \zeta}\, \mathrm{d}\zeta \,, \qquad j, l = 1, 2 \,; \quad j \neq l \,, \tag{8}$$

where (x_r, z_r) are the coordinates of the receiver. For $x_r > 0$, one can close the contour in the upper-half ζ-plane as $|\zeta| \to \infty$ and for $x_r < 0$ it can be closed in the lower half plane in the same limit. As follows we will take $x_r \geq 0$, corresponding to propagation in the positive x_r-direction. For this choice the contour must be displaced slightly above the real axis in the second quadrant and slightly below it in the fourth quadrant.

The dimensionless wave number $\kappa = (\omega/c_0)\, a$, where $a = \sqrt{c_0/c_2}$, is a large parameter of the problem even at moderate frequencies. For example, for the Munk canonical sound-speed profile [7] at the source frequency of 75 Hz, for the dimensionless wave number κ we get the value 2089.76. It means that for the functions $\Phi_1(z, \zeta)$ and $\Phi_2(z, \zeta)$ we can use their uniform asymptotic expansions as $\kappa \to \infty$ (see, for example, [8]). These asymptotics are expressed in terms of the parabolic cylinder functions $D_t(\pm\nu)$. The functions $D_t(\pm\nu)$ are defined so that as $|\nu| \to \infty$ we have (see Chap. 8 of [9] and Chap. 19 of [10])

$$D_t(\nu) \sim \mathrm{e}^{-\nu^2/4}\, \nu^t\, 2^{t/2} \left\{ 1 - \frac{t\,(t-1)}{2\,\nu^2} + \ldots \right\} \,, \qquad |\arg \nu| < \frac{3\pi}{4} \,; \tag{9}$$

$$D_t(-\nu) \sim \mathrm{e}^{-\nu^2/4}\, (-\nu)^t\, 2^{t/2} \left\{ 1 - \frac{t\,(t-1)}{2\,\nu^2} + \ldots \right\} \,, \qquad |\pi - \arg \nu| < \frac{3\pi}{4} \,. \tag{10}$$

The formulas relating $\Phi_j(z, \zeta)$ to $D_t(\pm\nu)$ as $k \to \infty$ are

$$\Phi_1(z, \zeta) \sim \frac{D_{\kappa\Delta - 1/2}\big(\sqrt{\kappa}\; \Xi(z, \zeta)\big)}{\sqrt{\Xi'(z, \zeta)}} \,, \tag{11}$$

$$\Phi_2(z, \zeta) \sim \frac{D_{\kappa\Delta - 1/2}\big(-\sqrt{\kappa}\; \Xi(z, \zeta)\big)}{\sqrt{\Xi'(z, \zeta)}} \,. \tag{12}$$

Here $\Xi(z, \zeta)$ is found from the implicit equation

$$\int\limits_{z^-(\zeta)}^{z} \sqrt{n^2(z) - \zeta^2}\; \mathrm{d}z = \int\limits_{-2\sqrt{\Delta}}^{\Xi(z,\zeta)} \sqrt{\Delta - \frac{s^2}{4}}\; \mathrm{d}s \,, \tag{13}$$

where

$$\Delta = \Delta(\zeta) = \frac{1}{\pi} \int\limits_{z^-(\zeta)}^{z^+(\zeta)} \sqrt{n^2(z) - \zeta^2}\; \mathrm{d}z \tag{14}$$

is the phase integral and $z^-(\zeta) < z^+(\zeta)$ are two roots of the equation $n^2(z) - \zeta^2 = 0$; $\Xi'(z, \zeta) = \partial\Xi(z, \zeta)/\partial z$.

We now consider the location of the singular points of the integrand in (8). Using the formula (see p. 687 of [10])

$$D_t(\nu)\, \frac{\mathrm{d}}{\mathrm{d}\nu} D_t(-\nu) - D_t(-\nu)\, \frac{\mathrm{d}}{\mathrm{d}\nu} D_t(\nu) = \frac{\sqrt{2\,\pi}}{\Gamma(-t)} \,,$$

where $\Gamma(-t)$ is the gamma function, we obtain for the Wronskian the following expression as $k \to \infty$

$$W(\zeta) \sim \sqrt{\frac{2\kappa}{\pi}}\; \Gamma(1 + t)\, \sin \pi t \tag{15}$$

with

$$t = t(\zeta) = \kappa\, \Delta(\zeta) - \frac{1}{2} \,. \tag{16}$$

Since the parabolic cylinder functions are entire functions of t, the integrand in (8) has simple poles only at the roots of the equation $\Gamma(1 + t)\, \sin \pi t = 0$ or at $\Gamma^{-1}(-t) = 0$, i.e. for

$$t = \kappa\, \Delta(\zeta) - \frac{1}{2} = m \,, \quad m = 0, 1, \ldots \,. \tag{17}$$

Because the expression $n^2(z) - \zeta^2$ includes ζ^2, the poles $\zeta = \pm\zeta_m$ are symmetric with respect to the origin in the ζ-plane. For $m \leq m_0$, where m_0 is some integer, the poles $\pm\zeta_m$ are real, whereas for $m > m_0$ they are purely imaginary.

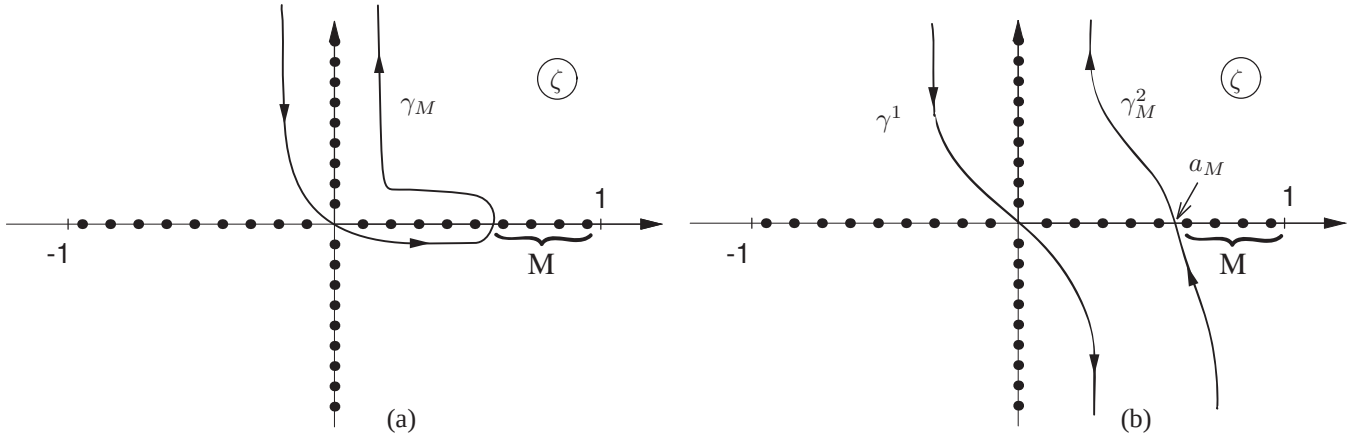

Fig. 3: (a) Integration contour γ_M in (19) and (b) the integration contours γ^1, γ_M^2. The poles of the integrand in (8) are presented by dots.

3 Transformation of the exact solution

Below we will examine in detail the case when the source and the observation point are located at the waveguide axis, i.e. $z_r = z_0 = 0$. Using asymptotic formulas for the parabolic cylinder functions $D_t(\pm\nu)$, it is possible to show that the integration contour in (8) can be deformed into the contour γ that surrounds the intervals $0 < \mathrm{Re}\,\zeta \leqslant 1$, $\mathrm{Im}\,\zeta = 0$ and $0 < \mathrm{Im}\,\zeta < +\infty$, $\mathrm{Re}\,\zeta = 0$. Then let us deform the integration contour γ in such a way to extract a sum of the first M residues of the integrand in (8) at the poles $+\zeta_m$, $m = 0, 1, \ldots, M-1 < m_0$; see Fig. 3 (a). These residues give us a sum of the first M propagating waveguide waves (normal modes). Selection of the value of M will be discussed later. As a result, (8) takes on the form

$$U(x_r, 0; 0) = \sum_{m=0}^{M-1} u_m^{\mathrm{mode}}(x_r, 0; 0) + I(x_r)\,, \qquad (18)$$

where

$$I(x_r) \sim \kappa \int\limits_{\gamma_M} \frac{D_t\big(\sqrt{\kappa}\;\Xi(0,\zeta)\big)\, D_t\big(-\sqrt{\kappa}\;\Xi(0,\zeta)\big)}{\Xi'(0,\zeta)\, W(\zeta)} \times \\ \times \exp\big(\mathrm{i}\,\kappa\, x_r\, \zeta\big)\,\mathrm{d}\zeta\,, \qquad (19)$$

$$u_m^{\mathrm{mode}}(x_r, 0; 0) \sim \frac{\sqrt{2}\;\pi^{3/2}\,\mathrm{i}\,(-1)^{m+1}}{\sqrt{\kappa}\; m!\,\zeta_m\,\Xi'(0,\zeta_m)} \times \\ \times \left(\int\limits_{z^-(\zeta_m)}^{z^+(\zeta_m)} \frac{1}{\sqrt{n^2(z) - \zeta_m^2}}\,\mathrm{d}z \right)^{-1} \exp\big(\mathrm{i}\,\kappa\, x_r\, \zeta_m\big) \times \\ \times D_m\big(\sqrt{\kappa}\;\Xi(0,\zeta_m)\big)\, D_m\big(-\sqrt{\kappa}\;\Xi(0,\zeta_m)\big) \qquad (20)$$

and t is given by (16).

In this paper we study the relationship between the first normal modes and the axial wave that describes the interference of the wave fields corresponding to rays having small launch angles with the wave travelling directly along the axis. In this case typically $M \leq 10$, and poles ζ_m are close to 1.

Now let us transform the integral (19). Using formulas from [10], it can be written as $k \to \infty$ in the form

$$I(x_r) \sim -\mathrm{i}\,\frac{\sqrt{\pi\,\kappa}}{2\sqrt{2}} \int\limits_{\gamma_M} G(\zeta)\, R(t)\, \frac{1 + \mathrm{e}^{\mathrm{i}\pi t}}{1 - \mathrm{e}^{\mathrm{i}\pi t}}\, \mathrm{e}^{\mathrm{i}\,\kappa\, x_r\, \zeta}\,\mathrm{d}\zeta\,, \qquad (21)$$

where

$$G(\zeta) = \frac{D_t\big(\sqrt{\kappa}\;\Xi(0,\zeta)\big)\, D_t\big(-\sqrt{\kappa}\;\Xi(0,\zeta)\big)}{\Xi'(0,\zeta)\, D_t^2(0)}\,, \qquad (22)$$

$$R(t) = 2^{-t}\,\frac{\Gamma(1+t)}{\Gamma^2(1+t/2)}\,. \qquad (23)$$

To investigate the behavior of the factor $R(t)$, we use the Stirling's formula (see p. 257 of [10]) to obtain the result as $|t| \to \infty$

$$R(t) \sim \begin{cases} \sqrt{2/\pi t}\;, & |\arg t| < \pi - \epsilon\,, \\ \mathrm{i}\,\sqrt{2/\pi t}\;\tan(\pi t/2)\,, & \epsilon < |\arg t| < 2\,\pi - \epsilon\,, \end{cases} \qquad (24)$$

where ε is an arbitrary positive constant.

On the integration contour γ_M we expand the function $\big(1 + \mathrm{e}^{\mathrm{i}\pi t}\big)/\big(1 - \mathrm{e}^{\mathrm{i}\pi t}\big)$ in a geometrical progression

$$\frac{1 + e^{\mathrm{i}\pi t}}{1 - e^{\mathrm{i}\pi t}} = 1 + 2\sum_{l=1}^{L-1} e^{\mathrm{i}\,\pi t l} + 2\,\frac{e^{\mathrm{i}\,\pi t L}}{1 - e^{\mathrm{i}\,\pi t}}\,. \qquad (25)$$

Selection of the value of L and the connection between M and L will be discussed later. The integrals

$$\int\limits_{\gamma_M} G(\zeta)\, R\,(t) \exp(\mathrm{i}\pi t l + \mathrm{i}\kappa x_r \zeta)\,\mathrm{d}\zeta$$

for $l = 0, 1, \ldots, L-1$ vanish since their integrands do not have singularities in the region to the left as one moves along the integration contour γ_M and they tend sufficiently fast to zero when $|\zeta| \to \infty$ in this region.

For the last term in (25), it does not exceed $|\exp\big(\mathrm{i}\pi t(L-1)\big)|$ in the upper half-plane and therefore the integral of this term along the contour γ_M will be convergent. Hence

$$I(x_r) \sim -\mathrm{i}\sqrt{\frac{\pi\,\kappa}{2}} \int\limits_{\gamma_M} G(\zeta)\, R(t)\, \frac{e^{\mathrm{i}\kappa\varphi_L(\zeta)}}{1-e^{\mathrm{i}\pi t}}\, \mathrm{d}\zeta\,, \qquad (26)$$

where we generally define

$$\varphi_L(\zeta) = \frac{\pi\, t\, L}{\kappa} + x_r\, \zeta\,. \qquad (27)$$

In (26) let us replace one integral along the contour γ_M by two integrals taken over γ^1 and γ_M^2, see Fig. 3 (b). The contour γ^1 begins at infinity in the sector $\pi/2 < \arg\zeta < 3\pi/4$ and it goes to infinity in the sector $-\pi/2 < \arg\zeta < -\pi/4$. The contour γ_M^2 begins at infinity in the sector $-\pi/2 < \arg\zeta < -\pi/4$ and it goes to infinity in the sector $\pi/4 < \arg\zeta < \pi/2$. The contour γ_M^2 crosses the real axis at $\zeta = a_M$, where

$$\zeta_M < a_M < \zeta_{M-1} \qquad (28)$$

and ζ_M is the M-th pole satisfying Eq. (17). Then

$$I(x_r) = I_L(x_r) + F_{L,M}(x_r)\,. \qquad (29)$$

Here as $k \to \infty$

$$I_L(x_r) \sim -\mathrm{i}\sqrt{\frac{\pi\,\kappa}{2}} \int\limits_{\gamma^1} G(\zeta)\, R(t)\, \frac{e^{\mathrm{i}\kappa\varphi_L(\zeta)}}{1-e^{\mathrm{i}\pi t}}\, \mathrm{d}\zeta\,, \qquad (30)$$

$$F_{L,M}(x_r) \sim -\mathrm{i}\sqrt{\frac{\pi\,\kappa}{2}} \int\limits_{\gamma_M^2} G(\zeta)\, R(t)\, \frac{e^{\mathrm{i}\kappa\varphi_L(\zeta)}}{1-e^{\mathrm{i}\pi t}}\, \mathrm{d}\zeta\,. \qquad (31)$$

It can be easily shown that the integrals (30) and (31) exist. In $I_L(x_r)$ we use

$$\frac{\exp(\mathrm{i}\pi t L)}{1-\exp(\mathrm{i}\pi t)} = \sum_{j=0}^{J-1} \exp\big(\mathrm{i}\pi t(L+j)\big) + \\ + \frac{\exp\big(\mathrm{i}\pi t(L+J)\big)}{1-\exp(\mathrm{i}\pi t)}\,. \qquad (32)$$

With this expansion it is possible to write the integral $I_L(x_r)$ as a sum of integrals

$$I_L = \sum_{j=0}^{J-1} s_{L+j} + S_{L+J}\,, \qquad (33)$$

where as $k \to \infty$

$$s_{L+j} \sim -\mathrm{i}\sqrt{\frac{\pi\,\kappa}{2}} \int\limits_{\gamma^1} G(\zeta)\, R(t)\, \exp\big(\mathrm{i}\,\kappa\,\varphi_{L+j}(\zeta)\big)\mathrm{d}\zeta\,, \qquad (34)$$

$$S_{L+J} \sim -\mathrm{i}\sqrt{\frac{\pi\,\kappa}{2}} \int\limits_{\gamma^1} \frac{G(\zeta)\, R(t)}{1-\exp(\mathrm{i}\,\pi\,t)}\, \exp\big(\mathrm{i}\,\kappa\,\varphi_{L+J}(\zeta)\big)\, \mathrm{d}\zeta\,. \qquad (35)$$

In the integral (34) the phase function $\varphi_{L+j}(\zeta)$ is given by (27); $G(\zeta)$ and $R(t)$, see (22), (23), are slowly varying functions, and for the function $R(t)$ the asymptotic formula (24) is valid. It means that the integral s_{L+j} can be evaluated by the method of steepest descent. As a result, we get

$$s_{L+j} = -\mathrm{i}\sqrt{\frac{\pi}{\kappa}}\, \frac{\exp(-\mathrm{i}\,(\pi/4)\,\mathrm{sign}\,b)}{\sqrt{|\pi\,(L+j) - x_r|}} \times$$

$$\times \exp\Big(\mathrm{i}\kappa\Big(x_r + \frac{\pi(L+j)}{2\,b}\Big(1 - \frac{x_r}{\pi(L+j)}\Big)^2\Big) - \mathrm{i}\frac{\pi}{2}(L+j)\Big)$$

$$\times \left\{1 + \mathrm{O}\Big(\frac{1}{\kappa(1-\hat\zeta_{L+j})}\Big) + \mathrm{O}\Big(\frac{1}{\kappa x_r |b| (1-\hat\zeta_{L+j})^2}\Big)\right\}\,, \qquad (36)$$

where

$$b = \frac{5}{8} - 3\,n_4 - \frac{15}{2}\,n_3^2 \qquad (37)$$

and $\hat\zeta_{L+j}$ is the saddle point that is found from the equation

$$x_r - \zeta(L+j) \int\limits_{z^-(\zeta)}^{z^+(\zeta)} \frac{\mathrm{d}z}{\sqrt{n^2(z) - \zeta^2}} = 0\,. \qquad (38)$$

In (36), the first error term is due to the use of the formula (24) for $R(t)$, whereas the second term specifies the error of the steepest descent method. The first term can be diminished if we retain in the asymptotic formula (24) not only the principal term, but correction terms as well. As to the second term, it will decrease with increasing $\kappa\, x_r$ if the following condition is imposed on the saddle point

$$|b|^{1/2}\,(1-\hat\zeta_{L+j}) > (\kappa\, x_r)^{-0.5+\delta}\,, \qquad (39)$$

where $\delta < 1/2$ is a fixed positive constant. Selection of the actual value of δ will be discussed later. For a wide range of x_r and κ this value is about 0.1. The inequality (39) will be correct for all $j = 0, 1, \ldots$, if

$$L > \frac{x_r}{\pi}\,\Big(1 + b^{1/2}\,(\kappa\, x_r)^{-0.5+\delta}\Big)\,, \quad \text{for} \quad b > 0 \qquad (40)$$

$$L < \frac{x_r}{\pi}\,\Big(1 - |b|^{1/2}\,(\kappa\, x_r)^{-0.5+\delta}\Big)\,, \quad \text{for} \quad b < 0\,. \qquad (41)$$

As it was shown in [4], if the inequalities

$$\frac{x_r}{\pi} < m \le \frac{x_r}{\pi}\,\Big(1 + b^{1/2}\big(\kappa x_r\big)^{-0.5+\delta}\Big)\,, \ \text{for} \ b > 0 \qquad (42)$$

$$\frac{x_r}{\pi}\,\Big(1 - |b|^{1/2}\big(\kappa x_r\big)^{-0.5+\delta}\Big) \le m < \frac{x_r}{\pi}\,, \ \text{for} \ b < 0 \qquad (43)$$

hold, the wave u_m with number m that crosses the waveguide axis at the observation point for the m-th time interferes with the wave u_0 propagating along the axis. If $b > 0$ the first to arrive is the perturbation that propagates along the

waveguide axis, and only after it do we get the waves that cross a certain (different) number of times the waveguide axis. In contrast, if $b < 0$ the wave travelling directly along the axis will be the last to arrive. Following to the definition given in [11], we get that if $b > 0$ the waveguide is abnormal and if $b < 0$ it is normal. In most long-range ocean propagation experiments, the deep-water waveguides are normal. Therefore, only normal waveguides will be considered below.

In terms of the ray method if the condition (41) is satisfied the applying of the steepest descent method to the integral s_{L+j} gives

$$s_{L+j} = \sqrt{\frac{2\pi}{\omega}}\,\exp\left(-\frac{\mathrm{i}\pi}{4}\right)\,\frac{1}{\sqrt{\widehat{J}_{L+j}}}\,\times \\ \times\exp\left\{\mathrm{i}\left(\omega\,T_{L+j}-\frac{\pi}{2}\,(L+j)\right)\right\}\times$$

$$\left\{1+\mathrm{O}\Big(\big(\kappa x_r\big)^{-\delta}\Big(\frac{|b|x_r}{\kappa}\Big)^{1/2}\Big)+\mathrm{O}\Big(\big(\kappa\,x_r\big)^{-2\delta}\Big)\right\}\,, \quad (44)$$

where the factor $\sqrt{2\pi/\omega}\,\exp(-\mathrm{i}\pi/4)$ characterizes the source, T_{L+j} is the propagation time of the wave u_{L+j} that arrives at the observation point $(x_r, 0)$ after $L+j$ intersections of the waveguide axis; $\hat{J}_{L+j}$ is the geometrical spreading.

It is evident that the integral $S_{L+J}(x_r)$, see (35), describes waves that cross the waveguide axis $L+J$ times and more.

The first goal of this paper is to obtain the representation of the acoustic field that includes ray summands, a sum of the first normal modes, and a remainder field. The condition (41) which ensures the applicability of the steepest descent method to the integrals s_{L+j} for $b < 0$ and obtaining Eq. (44) impose the following restriction on the point a_M where the integration contour γ_M^2 crosses the real axis (see Fig. 3 (b)):

$$\hat{\zeta}_{L-1} < a_M < \hat{\zeta}_L\,. \quad (45)$$

Here $\hat{\zeta}_L$ is the saddle point of the integral $s_L(x_r)$, see (38). As it was noted above, see (28), a_M must satisfy the inequalities

$$\zeta_M < a_M < \zeta_{M-1} \quad (46)$$

as well. Here ζ_M is the M-th pole of the integrand in (8).

It can be easily shown that under the condition (45) the integral $F_{L,M}(x_r)$, see (31), describing the remainder field, converges.

4 Relationship between the axial wave and the first normal modes

For the same medium model where the sound speed $c(Z)$ is given by the expression (1) the acoustic field can be represented in the form different from (18), (29). This representation includes ray summands corresponding to rays that arrive at the observation point after $L+j$, $j \geq 0$, intersections of the waveguide axis and the axial wave that describes the interference between the wave travelling along the axis and waves that propagate along other ray paths. The formula for the axial wave was obtained in [4].

If the waveguide is normal, i.e. the wave travelling along the waveguide axis is the last to arrive ($b < 0$), the value L is equal to N, where $N-1$ is the largest integer satisfying (41)

$$\frac{x_r}{\pi}\,\Big(1-|b|^{1/2}\,(\kappa\,x_r)^{-0.5+\delta}\Big) \leq N < \\ \frac{x_r}{\pi}\,\Big(1-|b|^{1/2}\,(\kappa\,x_r)^{-0.5+\delta}\Big)+1\,. \quad (47)$$

In this case the axial wave, $H_N(x_r)$, is given by the formula

$$H_N(x_r) = \sqrt{\frac{\pi}{2\kappa}}\,\exp\Big(-\mathrm{i}\,\frac{\pi}{2}(N+1)\Big)\times \\ \times\exp\left\{\mathrm{i}\Big(\kappa\,x_r-\frac{1}{8}\,(b-1+\frac{3}{4}\chi^2)\,\frac{x_r}{\kappa}\Big)\right\}\times \\ \times\int\limits_{\infty\exp(-3\mathrm{i}\pi/4)}^{\infty\exp(\mathrm{i}\pi/4)}\Lambda_N(\tau,x_r)\,\mathrm{d}\tau\left\{1+\mathrm{O}\Big(\frac{1}{\big(\kappa\,x_r\big)^{0.5-3\delta}}\Big)\right\}. \quad (48)$$

The integration in (48) begins at infinity in the complex τ-plane and goes to $\tau = 0$ along the straight line $\arg\tau = -3\pi/4$. From $\tau = 0$ it goes out to infinity along the straight line $\arg\tau = \pi/4$; $\chi = -4n_3/\sqrt{3}$.

A constant $0 < \delta < 1/2$ is selected in such a way to minimize the errors in computation of the integrals s_{N+j}, $j \geq 0$, see (44), and the error in computation of the axial wave $H_N(x_r)$.

The integrand in (48) is given by the formula

$$\Lambda_N(\tau,x_r) = 2^{-\tau}\,\frac{\Gamma(\tau+1/2)}{\Gamma^2\,(\tau/2+3/4)}\,\frac{\mathrm{e}^{\mathrm{i}\,\pi\,N\tau}}{1+\mathrm{i}\,\mathrm{e}^{\mathrm{i}\,\pi\,\tau}}\,\times \\ \times\,D_{\tau-1/2}\Big(\sqrt{\frac{2}{3}}\,\frac{\chi}{\sqrt{\kappa}}\,\tau\Big)\,D_{\tau-1/2}\Big(-\sqrt{\frac{2}{3}}\,\frac{\chi}{\sqrt{\kappa}}\,\tau\Big)\times \\ \times\,\big(D_{\tau-1/2}(0)\big)^{-2}\,\exp\left(-\mathrm{i}\,x_r\,\tau-\frac{\mathrm{i}}{2}\,b\,\frac{x_r}{\kappa}\tau^2\right)\,.$$

Comparing two representations of the acoustic field, we get that at $L = N$

$$H_N(x_r) = \sum_{m=0}^{M-1} u_m^{\mathrm{mode}}(x_r,0;0) + F_{L,M}(x_r)\,, \quad (49)$$

where M must satisfy the conditions (45), (46). Thus, the axial wave may alternatively be expressed by a group of the first normal modes plus a remainder. Although the remainder term contributes to the axial wave small amount of energy compared with a contribution of a cluster of the first modes, it cannot be neglected in order to represent accurately the axial wave.

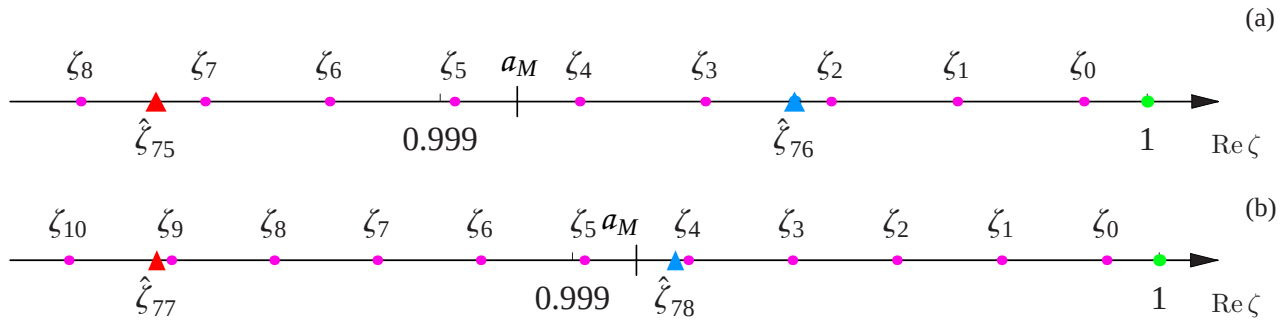

Fig. 4: The first 11 poles ζ_m of the integrand in (8) and two largest $\hat{\zeta}_m = \cos\psi_m$: (a) at the propagation range $X_r = 1600$ km and (b) at $X_r = 1650$ km.

The poles ζ_m of the integrand in (8) depend on frequency but do not depend on propagation range. In contrast, the saddle points $\hat{\zeta}_{L+j}$ of the integrals (34) depend on propagation range but do not depend on frequency. Thus, the number of normal modes in a cluster forming the axial wave depends on frequency, propagation range, and waveguide properties near the sound-channel axis (these properties specify the characteristic dimension of the waveguide, a, and parameters b and χ.

5 A numerical example

In most long-range ocean propagation experiments waveguides are normal. That is why as a numerical example we will consider the waveguide with the Munk canonical sound-speed profile [7, 11] which is the normal waveguide. In this case

$$c(Z) = c_0\Big(1 + \frac{1}{2}\,h\,\beta\,(\mathrm{e}^{2\,\xi} - 2\,\xi - 1)\Big)\,,$$

where

$$\xi = (Z - Z_0)/h\,,\quad \beta = 0.0113\times 10^{-3}\ \mathrm{m}^{-1}\,,$$

$$c_0 = 1500\ \mathrm{m/s}\,,\quad h = 1000\ \mathrm{m}\,,\quad Z_0 = -1000\ \mathrm{m}\,.$$

Then in the expansion for the index of refraction $n(z)$ we have $n_2 = 0.5$, $n_3 = -2.21730$, $n_4 = -7.12463$ and the main parameters of the problem will be as follows

$$a = 6651.90\ \mathrm{m}\,,\quad b = -14.87430\,,\quad \chi = 5.12064\,.$$

Let us take the source frequency, f, equal to 200 Hz. Then $\omega = 400\,\pi\ \mathrm{s}^{-1}$ and for the dimensionless wave number κ we get the value $\kappa = (\omega/c_0)\,a = 5572.68$.

The acoustic field will be computed for the propagation ranges $1600 \le X_r \le 1650$ km (or for the dimensionless distances $240.533 \le x_r \le 248.049$).

A constant $0 < \delta < 1/2$ is selected in such a way to minimize the errors in computation of the integrals s_{N+j}, $j \ge 0$, see (44), and the error in computation of the axial wave $H_N(x_r)$, see (48). As a result, we get $\delta = 0.101502$.

For the medium model described above the first poles ζ_m, $m = 0, 1, \ldots$ of the integrand in (8), see (17), (14), are

$$\zeta_0 = 0.999910\,,\quad \zeta_1 = 0.999731\,,\quad \zeta_2 = 0.999553\,,$$
$$\zeta_3 = 0.999375\,,\quad \zeta_4 = 0.999197\,,\quad \zeta_5 = 0.999020\,,$$
$$\zeta_6 = 0.998844\,,\quad \zeta_7 = 0.998667\,,\quad \zeta_8 = 0.998492\,,$$
$$\zeta_9 = 0.998316\,,\quad \zeta_{10} = 0.998142\,.$$

The saddle points $\widehat{\zeta}_m$, see (38), depend on x_r. The ray, arriving at the observation point $(x_r, 0)$ after m intersections of the waveguide axis, has the launch angle $\Psi_m = \arccos\widehat{\zeta}_m$, $m \le x_r/\pi$. The wave u_m corresponding to this ray interferes with the wave u_0 travelling directly along the axis ($\Psi = 0$) if the inequalities (43) are satisfied. For the considered medium model at $X_r = 1600$ km there is only one wave u_{76} interfering with u_0; $\widehat{\zeta}_{76} = 0.999501$; see Fig. 4 (a). The preceding $\widehat{\zeta}_{75} = 0.998598$ corresponds to the wave u_{75} that is observed independently of u_0.

At $X_r = 1650$ km the situation is similar: there is the only interfering wave u_{78}; $\widehat{\zeta}_{78} = 0.999176$. The wave u_{77} does not interfere with the wave u_0 propagating along the waveguide axis; $\widehat{\zeta}_{77} = 0.998292$; see Fig. 4 (b).

For the propagation ranges $1600 \le X_r \le 1650$ km the constant a_M can be chosen as the middle of the interval (ζ_5, ζ_4), i.e. we put $M = 5$. In this case to the right of a_M there will be the single $\hat{\zeta}_m$ corresponding to the interfering wave and to the left of a_M – only $\hat{\zeta}_m$ corresponding to the waves u_m that do not participate in the interference process.

Let $N - 1$ be the largest integer satisfying (41); see (47). $N = 76$ if $1600 \le X_r \le 1610$ km, $N = 77$ if $1610 \le X_r \le 1631.2$ km, and $N = 78$ if $1631.2 \le X_r \le 1650$ km. If a_M is chosen so that $\zeta_5 < a_M < \zeta_4$, then $L = N$, where $\hat{\zeta}_{L-1} < a_M < \hat{\zeta}_L$, see (45), and as it has been shown in this paper, the equality (49) is satisfied.

In Fig. 5 and 6 one can see a graph of the magnitude of the axial wave $|H_N(x_r)|$, a graph of the magnitude of a sum of the first five normal modes and a graph of $\Big|\sum_{m=0}^{4} u_m^{\mathrm{mode}}(x_r, 0; 0) + F_{L,M}(x_r)\Big|$ as functions of dimensional propagation range X_r in the interval $1600 \le X_r \le 1650$ km. Figures 5 and 6 show that the axial wave cannot be represented as a sum of the first five normal modes, but taking into account the remainder field $F_{L,M}(x_r)$, we get the very close concordance.

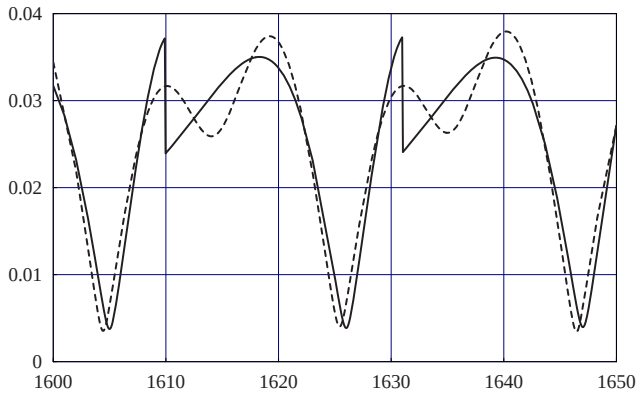

Fig. 5: Plots of $|H_N(x_r)|$ (solid line), $|\sum_{m=0}^{4} u_m^{\mathrm{mode}}(x_r,0;0)|$ (dashed line) as functions of dimensional propagation range X_r in the interval $1600 \le X_r \le 1650$ km.

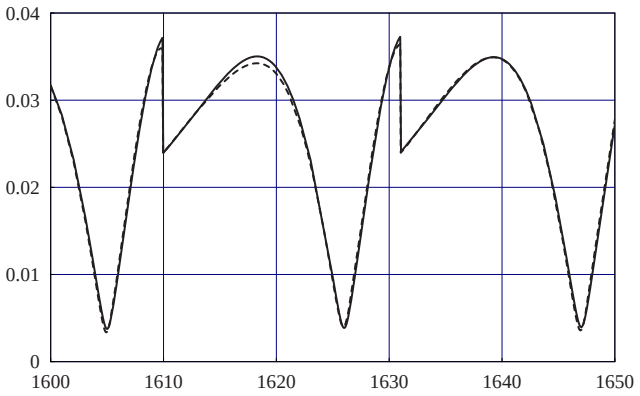

Fig. 6: Plots of $|H_N(x_r)|$ (solid line) and $|\sum_{m=0}^{4} u_m^{\mathrm{mode}}(x_r,0;0) + F_{L,M}(x_r)|$ (dashed line) as functions of dimensional propagation range X_r in the interval $1600 \le X_r \le 1650$ km.

The constant a_M could be chosen in another way. For the whole propagation range we could take a_M equal to the middle of the interval (ζ_6, ζ_5) putting $M = 6$, but in this case the magnitude of the remainder increases. It means that for the considered medium model the "optimum" number of modes in a cluster is equal to five.

Comparing at $X_r = 1600$ km the propagation times for the first five modes

$$t_0 = 1066.66661 \text{ s}, \quad t_1 = 1066.66609 \text{ s},$$

$$t_2 = 1066.66509 \text{ s},$$

$$t_3 = 1066.66359 \text{ s}, \quad t_4 = 1066.66159 \text{ s}$$

with the propagation time for the group of these interfering modes forming an axial wave

$$t_{\mathrm{ax}} = 1066.66668 \text{ s},$$

we see that the group of interfering modes arrives at the observation point simultaneously with the slowest mode.

6 Conclusions

In many long-range propagation experiments the source and receiver are placed close to the depth of the waveguide axis. The time-of-arrival patterns of these experiments consist of resolvable, geometrical-like arrivals followed by an axial crescendo of unresolved energy. It is impossible to explain this late-arriving energy using the geometrical acoustics because of the presence of cusped caustics repeatedly along the waveguide axis. The interference of the wave fields corresponding to the rays located in the vicinity of the caustics near the waveguide axis produces a special "axial wave" that propagates along the axis.

There is, however, another well-known representation of the acoustic field in terms of propagating and decaying modes. In this paper the relationship has been studied between the first modes and the axial wave. Along with the representation of the acoustic field as a sum of ray summands and the axial wave one more representation of the acoustic field has been derived in this paper. It includes a sum of the first normal modes, ray summands, and a remainder field. Comparing these two representations, it has been shown that the axial wave may alternatively be expressed by a well-specified group of the first normal modes plus the remainder. Although the remainder term contributes to the axial wave small amount of energy compared with the contribution of the sum of the first modes, it cannot be neglected in order to represent accurately the axial wave.

This conclusion was verified by numerical computations that have been carried out for the normal waveguide with the Munk canonical sound-speed profile in the range interval $1600 \le X_r \le 1650$ km; $f = 200$ Hz. For the considered medium model the axial wave is represented by a group of the first 5 or 6 normal modes plus the remainder. The requirement of minimization of the remainder defines the "optimum" choice of the number of modes in the cluster. This number is equal to five.

The number of normal modes in a cluster forming the axial wave depends on frequency, propagation range, and the waveguide properties near the waveguide axis. Comparison of arrival times for the first five normal modes with the arrival time of the axial wave shows that the axial wave arrives simultaneously with the slowest mode. Thus, using the representation of the axial wave in the form of a sum of the first normal modes and a remainder, it is possible to separate the group of modes that are detected at the observation point as a "single" perturbation with the arrival time almost coinciding with the arrival time of the slowest mode.

7 Acknowledgments

This research was supported by the Department of the Navy, Office of Naval Research (code 321 OA).

References

[1] P.F. Worcester et al., "A test of basin-scale acoustic thermometry using a large-aperture vertical array at 3250-km range in the eastern North Pacific Ocean", *J. Acoust. Soc. Am.* 105, 3185–3201 (1999)

[2] T. Pearcey, "The structure of an electromagnetic field in the neighborhood of a cusp of a caustic", *Philos. Magazine*, 37, 311–317 (1946)

[3] V.S. Buldyrev, "The field of a point source in a waveguide", *Trudy Mat. Inst. Steklov.* 115, 78–102 (1971) in Russian

[4] N.S. Grigorieva and G.M. Fridman, "Axial wave in long-range propagation in a range-independent ocean", *J. Comp. Acoust.* 12, 127 -147 (2004)

[5] N.S. Grigorieva and G.M. Fridman, "Effect of horizontal inhomogeneity of the ocean on interference of near-axial waves in long-range acoustic propagation", *J. Comp. Acoust.* 14, 415–443 (2006)

[6] N.S. Grigorieva and G.M. Fridman, "Relationship between the axial wave and first normal modes for ducted propagation in a waveguide", *J. Comp. Acoust.* 16, 117–135 (2008)

[7] W.H. Munk, "Sound channel in an exponentially stratified ocean, with application to SOFAR", *J. Acoust. Soc. Am.* 55, 220–226 (1974)

[8] D.S. Ahluwalia and J.B. Keller, "Exact and asymptotic representation of the sound field in a stratified ocean", in *Wave Propagation and Underwater Acoustics, Lecture Notes in Physics*, eds. J.B. Keller and J.S. Papadakis (Springer Verlag, Berlin, Heidelberg, 1977).

[9] H. Bateman and A. Erdélyi, *Higher Transcendental Functions*, Vol. **2** (McGraw Hill Book Company, New York, Toronto, 1953).

[10] *Handbook of Mathematical Functions*, eds. M. Abramovitz and I. Stegun (Dover Publications, Inc., New York, 1970).

[11] W.H. Munk, P.F. Worcester, and C. Wunsch, *Ocean Acoustic Tomography* (Cambridge U.P., London, 1995).